Thermal expansion, heat capacity and magnetostriction of RAl_3 (R = Tm, Yb, Lu) single crystals

2008 J. Phys.: Condens. Matter 20 025220

(http://iopscience.iop.org/0953-8984/20/2/025220)

J. Phys.: Condens. Matter **20** (2008) 025220 (8pp) doi:10.1088/0953-8984/20/02/025220

Thermal expansion, heat capacity and magnetostriction of RAl_3 (R = Tm, Yb, Lu) single crystals

S L Bud'ko[1], J C Frederick[1], E D Mun[1], P C Canfield[1] and G M Schmiedeshoff[2]

[1] Ames Laboratory US DOE and Department of Physics and Astronomy, Iowa State University, Ames, IA 50011, USA
[2] Department of Physics, Occidental College, Los Angeles, CA 90041, USA

Received 24 September 2007, in final form 2 November 2007
Published 13 December 2007
Online at stacks.iop.org/JPhysCM/20/025220

Abstract

We present thermal expansion and longitudinal magnetostriction data for cubic RAl_3 (R = Tm, Yb, Lu) single crystals. The thermal expansion coefficient for $YbAl_3$ is consistent with an intermediate valence of the Yb ion, whereas the data for $TmAl_3$ show crystal electric field contributions and have strong magnetic field dependences. de Haas–van Alphen like oscillations were observed in the magnetostriction data for $YbAl_3$ and $LuAl_3$, several new extreme orbits were measured and their effective masses were estimated. Specific heat data taken at 0 and 140 kOe for both $LuAl_3$ and $TmAl_3$ for $T \leqslant 200$ K allow for the determination of a crystal electric field splitting scheme for $TmAl_3$.

(Some figures in this article are in colour only in the electronic version)

1. Introduction

Rare earth trialuminides, RAl_3, have been studied for several decades. The crystal structure of these materials is very sensitive to the rare earth ionic radius and it changes from hexagonal for light rare earths to cubic (Cu_3Au type) for $TmAl_3$, $YbAl_3$, $LuAl_3$ (and $ScAl_3$) [1], with $ErAl_3$ reported to have been synthesized in both crystallographic variants [1–3]. $TmAl_3$ was reported to have a singlet ground state [3, 4]: the magnetic susceptibility follows the Curie–Weiss law with the magnetic moment corresponding to that of Tm^{3+} at high temperatures and becomes of temperature independent Van Vleck type at low temperatures. $YbAl_3$, an intermediate valence compound [5] with the high Kondo temperature, T_K, of 600–700 K, recently experienced a revival of interest in its physical properties [6–10] based, in part, on the uncovering of a second, low temperature, energy scale, Fermi liquid coherence ($T_{coh} \approx 40$ K), and slow crossover between T_K and T_{coh} [11].

Whereas many physical properties were measured and analyzed for cubic trialuminides, thermal expansion and magnetostriction data for these materials, in particular at low temperatures, appear to be absent from the literature (except for an early report [12] on the thermal expansion of $LuAl_3$ and $YbAl_3$ between ~90 and ~800 K). In addition, for $TmAl_3$, the exact crystal electric field (CEF) splitting of the Hund's rule ground state multiplet has remained unresolved [4, 13–15], in part due to a lack of high temperature and high magnetic field specific heat data. In this work we report extensive measurements of specific heat as well as thermal expansion and magnetostriction data for RAl_3 (R = Tm, Yb, Lu) single crystals so as to allow comparison with other salient physical properties and to inquire into the effects of the CEF and intermediate valence (IV) on these characteristics. Simple crystal structure and the ability to synthesize large, high quality, single crystals facilitate this endeavor.

2. Experimental methods

Large (>0.1 cm^3) single crystals (figure 1, inset) of RAl_3 (R = Tm, Yb, Lu) and $R'_{0.1}Lu_{0.9}Al_3$ (R′ = Er, Tm, Yb) were grown from aluminum-rich binary (R–Al) or ternary (R′–Lu–Al) melts using a self-flux method [16]. High purity R (Ames Lab) and Al were placed, in atomic ratios of $R_{0.12}Al_{0.88}$ or $(Lu_{0.9}R_{0.1})_{0.12}Al_{0.88}$, in alumina crucibles. These were sealed in fused quartz ampoules under a 1/3 atmosphere partial pressure of Ar. The ampoules were heated to 1050 °C and then cooled to 675 °C over 150–160 h, at which point

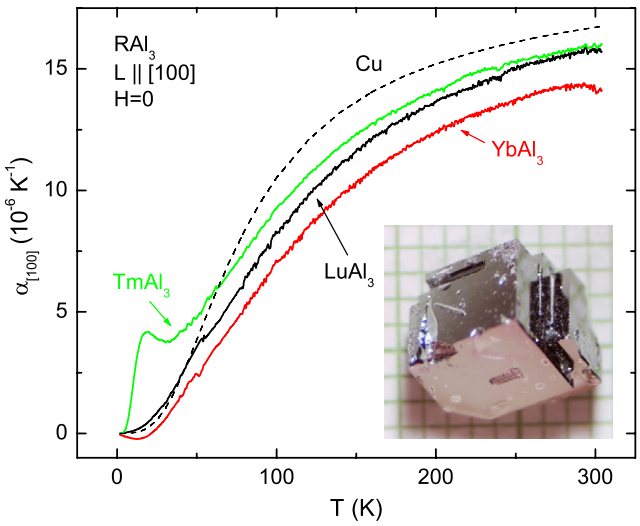

Figure 1. Temperature dependent linear thermal expansion coefficients along the [100] direction of RAl_3 (R = Tm, Yb, Lu) in zero applied field. Data for polycrystalline Cu [19] are shown as a dashed line for comparison. Inset: $LuAl_3$ crystal over a mm scale.

they were removed from the furnace and the excess Al was decanted. For $R'_{0.1}Lu_{0.9}Al_3$ with R′ = Er, Tm the nominal concentration of R′ was corroborated by the Curie–Weiss fit of the high temperature susceptibility. The inset to figure 1 shows crystals with clear, cubic morphology and mirrored (100) facets. Linear dimensions as large as 7 mm were commonly achieved. The quality of the crystals is attested by e.g. an absence of the low temperature Curie tail (caused by impurities) in the low field magnetic susceptibility of $YbAl_3$ (the data are similar to those reported in [6]), and observation of quantum oscillations up to temperatures as high as 20 K (see below).

Thermal expansion and magnetostriction were measured using a capacitive dilatometer constructed of OFHC copper; a detailed description of the dilatometer is presented elsewhere [17]. The dilatometer was mounted in a Quantum Design PPMS-14 instrument and was operated over a temperature range of 1.8–300 K in an applied magnetic field up to 140 kOe. The samples were mounted in such a way that thermal expansion was measured along the [100] direction. The applied magnetic field was also along [100] such that $H \parallel L \parallel [100]$. The crystals were cut and polished so that the typical distance between the parallel (100) surfaces of the samples was $L_{[100]} \approx$ 2–3 mm. The heat capacity of the samples was measured using a hybrid adiabatic relaxation technique with the heat capacity option in a Quantum Design PPMS-14.

Thermodynamic properties of materials are frequently analyzed using the concept of a Grüneisen function (or a Grüneisen parameter) [18]. For a single salient energy scale, ε, the Grüneisen parameter, γ, is defined as $\gamma = -\mathrm{d}\ln\varepsilon/\mathrm{d}\ln V$, where V is a molar volume. Using thermodynamic relations, we can obtain $\gamma(T, V) = \beta V/\chi_S C_\mathrm{p}$, where β is a volume thermal expansion coefficient ($\beta = (\partial \ln V/\partial T)_P$), χ_S is an adiabatic compressibility ($\chi_S = -(\partial \ln V/\partial P)_S$) and C_p is a heat capacity at a constant pressure. For cubic materials $\gamma(T, V) = 3\alpha V/\chi_S C_\mathrm{p}$, where α is a linear thermal expansion coefficient ($\alpha = (\partial \ln a/\partial T)_P$, a is a lattice parameter). Sometimes, in the analysis of experimental data, lacking the temperature dependent compressibility data, the temperature dependence of the Grüneisen parameter can be approximated [20] as being proportional to β/C_p (or $3\alpha/C_\mathrm{p}$ for cubic materials) under the assumption that the relative temperature dependence of χ_S is significantly smaller then that of the thermal expansion coefficient or heat capacity. We will adopt such an approach in this work.

If more than one contribution to the thermodynamic properties is present (e.g. vibrational, electronic, magnetic, etc), the Grüneisen parameters are not additive; rather the Grüneisen parameter for the material is an average, weighted by the heat capacity contributions of each of the components [18]: $\gamma = \sum_r \gamma_r C_r / \sum_r C_r$.

3. Results and discussion

3.1. Thermal expansion and heat capacity

Zero field, temperature dependent, linear ($L \parallel [100]$) thermal expansion coefficients for RAl_3, where R = Tm, Yb, Lu (together with the literature data [19] for polycrystalline Cu for comparison), are shown in figure 1. In the overlapping temperature regions ($T > 90$ K), the thermal expansion coefficient values for $LuAl_3$ and $YbAl_3$ deduced from the lattice parameters as a function of temperature data [12] are comparable to our results. At room temperature, thermal expansion values of the non-hybridizing $TmAl_3$ and $LuAl_3$ are very similar. The differences in $\alpha(T)$ between these two materials, on cooling, and in particular a peak in $\alpha(T)$ of $TmAl_3$ at ∼20 K, are probably related to the CEF contributions to the thermal expansion of $TmAl_3$. $\alpha(T)$ for $YbAl_3$ is lower than that for its non-magnetic analog, $LuAl_3$, over the whole temperature range. Such behavior is consistent [21] with $YbAl_3$ being an Yb-based, intermediate valence material with a high, $T_\mathrm{K} \gg 300$ K, Kondo temperature. Qualitatively, such behavior can be understood by noting that the fractional Yb valence in $YbAl_3$ increases with increase in temperature (in the temperature range of our measurements) [22] and that the ionic radius of Yb^{3+} is smaller than that of Yb^{2+}.

Figure 2 presents the temperature dependent linear thermal expansion coefficient (α), the heat capacity (C_p) and the ratio α/C_p for $LuAl_3$. $\alpha_{[100]}(T)$ and $C_\mathrm{p}(T)$ have similar temperature dependences. The ratio of these two quantities (that, as mentioned above, is likely to approximate the temperature dependence of the Grüneisen parameter) is practically constant down to ∼50 K, only rising at lower temperatures and manifesting a peak at ∼8 K. It is not unusual to observe a temperature dependent Grüneisen parameter, even for simple, non-magnetic, metals [18]. This is due to the different temperature dependences of the electron and phonon contributions to the thermodynamic properties, with these contributions becoming comparable in magnitude at low temperatures. Additionally, the error bars in α/C_p may be somewhat enhanced at low temperatures as a result of calculating the ratio of two, diminishingly small numbers.

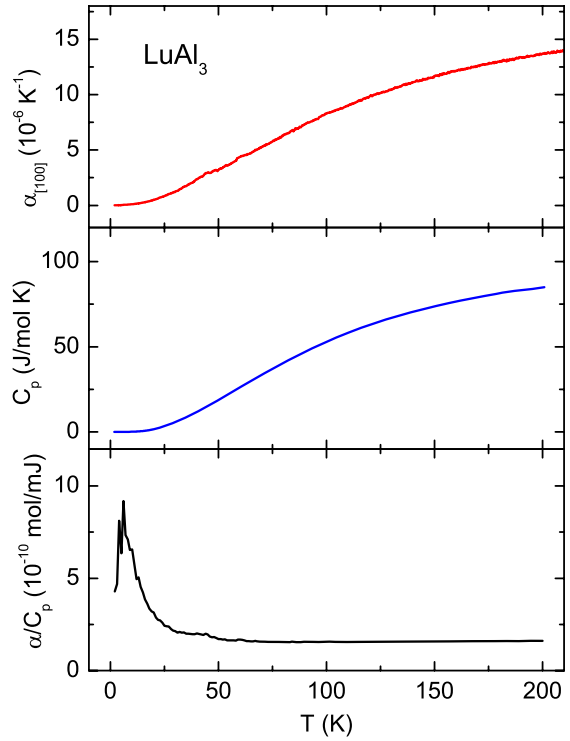

Figure 2. Temperature dependent linear thermal expansion coefficient, heat capacity and the ratio α/C_p for $LuAl_3$ in zero applied field.

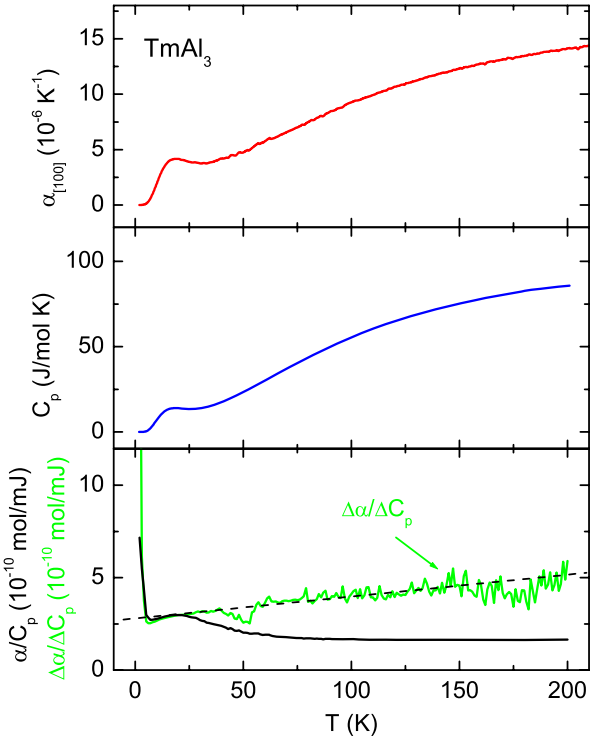

Figure 3. Temperature dependent linear thermal expansion coefficient, heat capacity and the ratio α/C_p for $TmAl_3$ in zero applied field. Additionally, in the lower panel $\Delta\alpha/\Delta C_p = (\alpha(TmAl_3) - \alpha(LuAl_3))/(C_p(TmAl_3) - C_p(LuAl_3))$ is plotted. The dashed line is a guide for the eye.

For $TmAl_3$ (figure 3) both thermal expansion and heat capacity exhibit a broad peak in the 15–20 K temperature range, apparently related to CEF effects. This peak is still observable in the α/C_p curve; however, if the data are plotted as $\Delta\alpha/\Delta C_p$ (i.e. after subtraction of the non-magnetic background) it is not seen, confirming the same origin of the feature in C_p and α. $\Delta\alpha/\Delta C_p$ shows a close to linear, slowly changing with temperature, behavior, probably representing rather well the behavior of the magnetic contribution to the Grüneisen parameter.

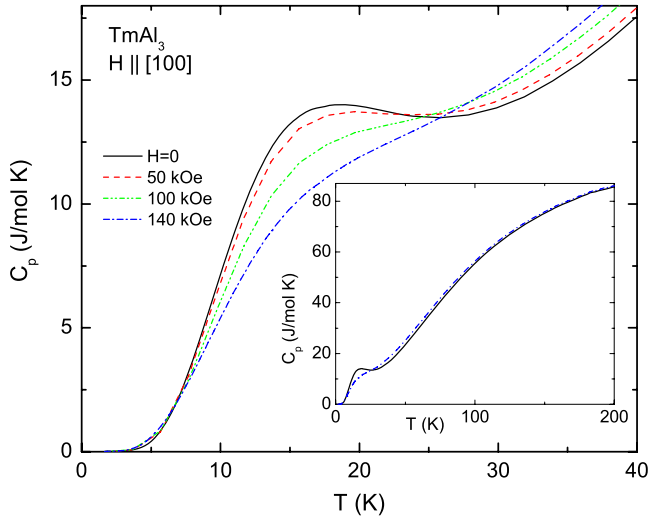

Figure 4. The low temperature part of the heat capacity for $TmAl_3$ in applied fields $H = 0, 50, 100, 140$ kOe. The field was applied along the [100] axis. Inset: data for $H = 0$ and 140 kOe up to 200 K.

The peak in heat capacity evolves with applied field (figure 4) reflecting the lifting of the degeneracy of $TmAl_3$ energy levels. A variety of differing CEF schemes, based on fits of different experimental quantities ($C_p(T)$, or $\chi(T)$, or high field $M(H)$) were suggested for $TmAl_3$ in the literature [4, 13–15]. To analyze our magnetization, susceptibility and specific heat data we will use the approach delineated in [23]. Since Tm^{3+} ions in $TmAl_3$ have the octahedron type of coordination, both parameters, W and x, of the CEF Hamiltonian for cubic symmetry (see [23] for definitions of these parameters and detailed discussion) are negative and the ground state is Γ_2 (set 1) or Γ_1 (set 2). Temperature dependent susceptibility and magnetization isotherms up to 70 kOe (figure 5) allow for similar quality fits for CEF schemes with either ground state. Heat capacity data are better fit with the CEF scheme corresponding to Γ_2 ground state (figure 6) (for both sets the W and x values from fits of temperature dependent susceptibility and magnetic isotherms were used). The W and x values for both sets are listed on the graph. An applied magnetic field changes the CEF splitting via the Zeeman term. The $H = 0$ CEF levels plus this Zeeman term describe $H = 140$ kOe data well (figure 6).

Figure 7 shows the simulation of the heat capacity behavior using the various CEF splitting schemes proposed in the literature [4, 13–15] including two of the three schemes [4] presented as indistinguishable given their low temperature data. Set 2 in [4] and the parameters from [13] are close to our results (set 1) and describe the heat capacity data reasonably

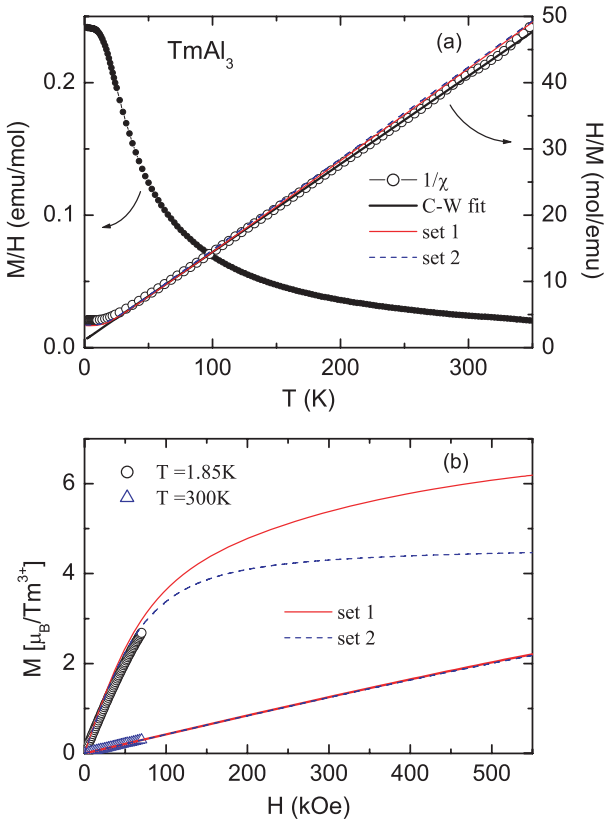

Figure 5. (a) Temperature dependent magnetic susceptibility, M/H, inverse magnetic susceptibility, H/M, taken at $H = 1$ kOe, $H \parallel [100]$ and (b) magnetization isotherms, $M(H)$, for $T = 1.85$ and 300 K for $TmAl_3$. The Curie–Weiss fits of the inverse magnetic susceptibility and CEF simulations of H/M and $M(H)$ for two possible sets of parameters (set 1: $W = -1.011$, $x = -0.298$ set 2: $W = -2.125$, $x = -0.682$) are shown as lines.

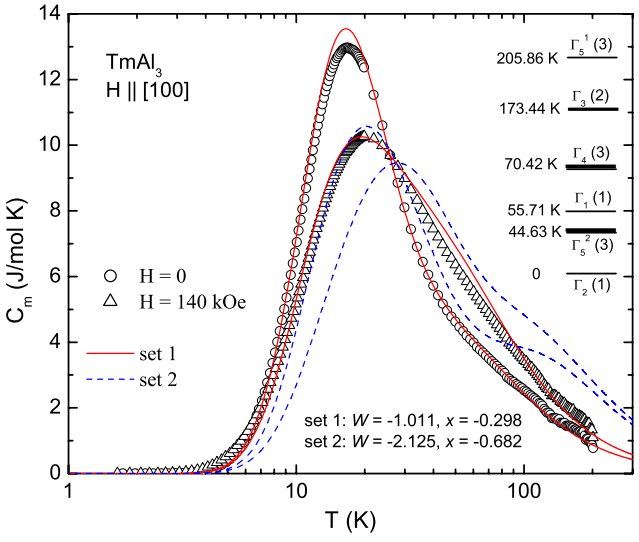

Figure 6. Magnetic contribution to the heat capacity of $TmAl_3$, $C_m = C_p^{TmAl_3} - C_p^{LuAl_3}$, in zero and 140 kOe ($H \parallel [100]$) applied field. CEF simulations for two possible sets of parameters are show as lines. Corresponding W and x values are listed for both sets. The CEF scheme for set 1 is illustrated on the right side of the plot.

well, whereas the parameters from [14, 15] and set 1 in [4] fail as reasonable approximations of the experimental data.

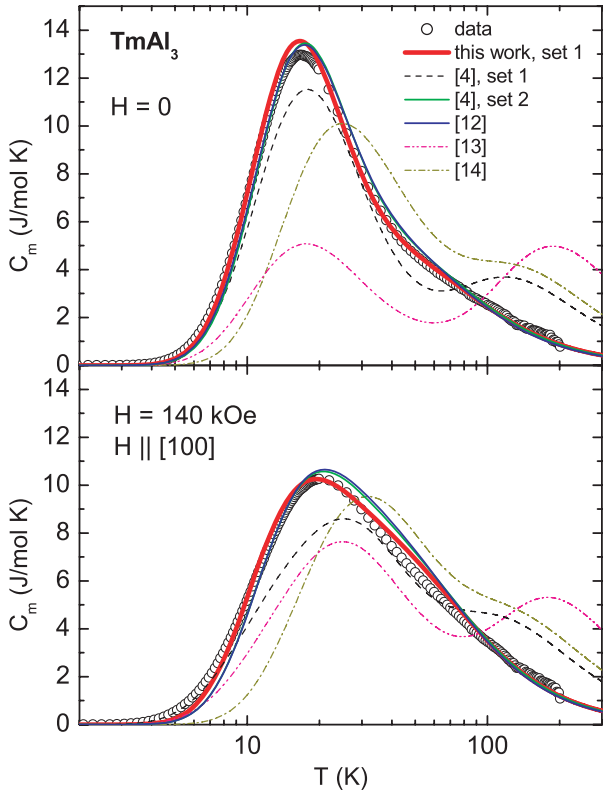

Figure 7. Magnetic contribution to the heat capacity of $TmAl_3$, $C_m = C_p^{TmAl_3} - C_p^{LuAl_3}$, in zero and 140 kOe ($H \parallel [100]$) applied field. CEF simulations using set 1 from this work and the literature data are shown as lines. The following W and x values (listed as $\{W, x\}$) were used: this work, set 1: $\{-1.011, -0.298\}$; reference [4], set 1: $\{1.95, 0.82\}$, set 2: $\{-0.993, -0.282\}$; reference [13]: $\{-0.94, -0.27\}$; reference [14]: $\{3.24, -0.8\}$; reference [15]: $\{-2.316, -0.827\}$.

An applied field changes the behavior of the thermal expansion coefficient of $TmAl_3$ dramatically (figure 8). In between 25 and 50 kOe the low temperature maximum turns into a minimum. This minimum deepens in higher fields and reaches $\approx -1.7 \times 10^{-5}$ K^{-1} near 15 K for $H = 140$ kOe. Clearly, as a result of the changing CEF energy scales, the Grüneisen parameter will be significantly different in the applied field. Qualitatively similar, but approximately an order of magnitude lower in size, field-induced changes in $\alpha_{[100]}(T)$ are observed in $Tm_{0.1}Lu_{0.9}Al_3$ (cf two insets to figure 8). These perceptible field dependences of $\alpha_{[100]}(T)$ in both $TmAl_3$ and $Tm_{0.1}Lu_{0.9}Al_3$ are consistent with a CEF-related, single-ion effect.

To illustrate the complexity of the effect of magnetic field on the thermal expansion coefficient, data for $Er_{0.1}Lu_{0.9}Al_3$ are shown in figure 9. As opposed to the case for $Tm_{0.1}Lu_{0.9}Al_3$ (figure 8, inset) a *positive*, broad feature in $\alpha_{[100]}(T)$ below ~40 K grows with increasing applied magnetic field. Transverse thermal expansion measurements in an applied field and some knowledge of the CEF scheme for $Er_{0.1}Lu_{0.9}Al_3$ would be needed for comparative analysis of the effects of magnetic field on these two different materials.

For $YbAl_3$, $\alpha_{[100]}(T)$ and $C_p(T)$ (figure 10) have similar temperature dependences, without any apparent striking

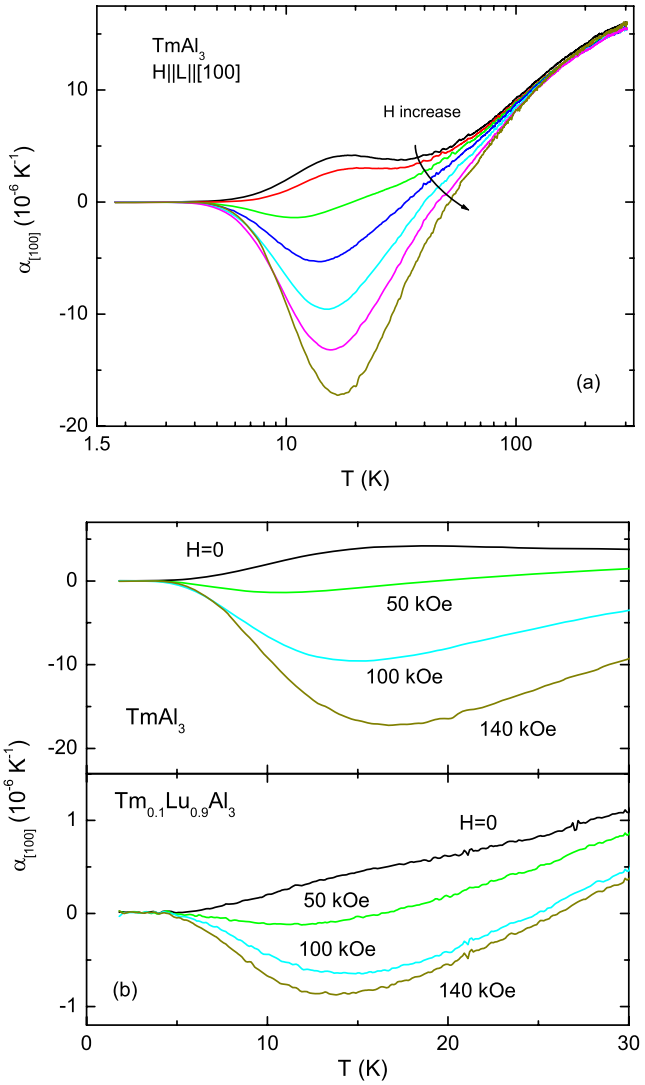

Figure 8. (a) Temperature dependent linear thermal expansion coefficient for $TmAl_3$ in applied fields of 0, 25, 50, 75, 100, 125, 140 kOe. (b) Low temperature part of $\alpha(T)$ in 0, 50, 100, 140 kOe applied fields for $TmAl_3$ and $Tm_{0.1}Lu_{0.9}Al_3$.

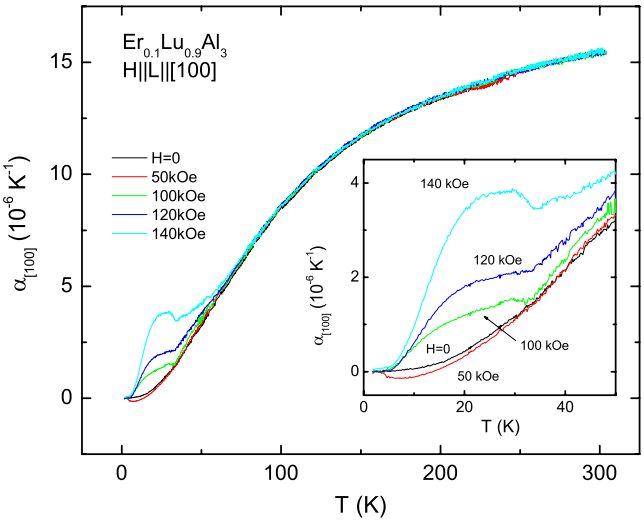

Figure 9. Temperature dependent linear thermal expansion coefficient for $Er_{0.1}Lu_{0.9}Al_3$ in applied fields of 0, 50, 100, 120, 140 kOe. Insets: the low temperature part of $\alpha(T)$.

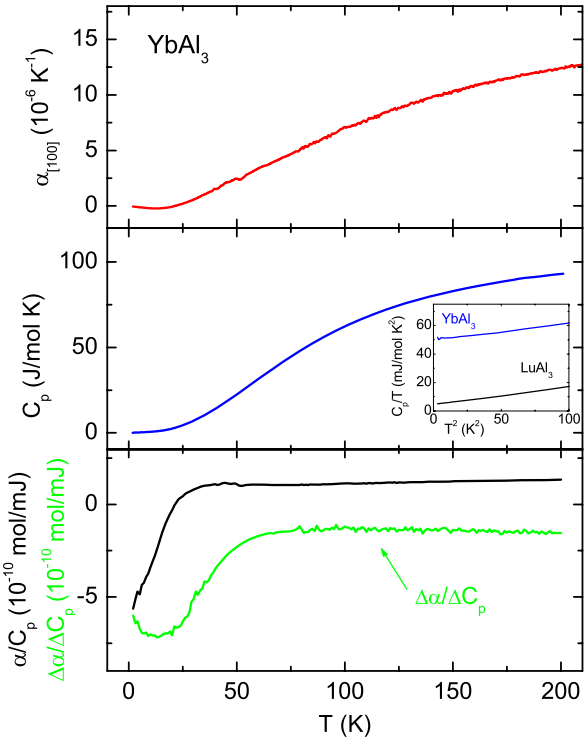

Figure 10. Temperature dependent linear thermal expansion coefficient, heat capacity and the ratio α/C_p for $YbAl_3$ in zero applied field. Additionally, in the lower panel $\Delta\alpha/\Delta C_p = (\alpha(YbAl_3) - \alpha(LuAl_3))/(C_p(YbAl_3) - C_p(LuAl_3))$ is plotted. Inset: low temperature C_p/T versus T^2 for $LuAl_3$ and $YbAl_3$.

features. The ratio of these two quantities is practically constant down to ∼30 K and then decreases at lower temperatures. $\Delta\alpha/\Delta C_p$ is linear (and close to constant) at higher temperatures and then, on further cooling, decreases and passes through a broad minimum. Given that the Kondo temperature is above room temperature [5], it is tempting to try to connect these changes in $\Delta\alpha/\Delta C_p$ to the emerging second, low temperature (∼30–40 K), scale for $YbAl_3$ [11]; however at this point there is no clear evidence for such a conjecture and more studies are required. Additionally, we cannot exclude the possibility of this low temperature behavior being the result of an interplay between phonons and (enhanced) electronic degrees of freedom. Specific heat data show an elevated electronic specific heat coefficient, $\gamma \sim 50$ mJ mol^{-1} K^{-2}, for $YbAl_3$, significantly higher than that for $LuAl_3$, consistently with the intermediate valence nature of $YbAl_3$, similarly to recently reported data [24].

$\alpha_{[100]}(T)$ for $YbAl_3$ is not significantly affected by an applied magnetic field of 140 kOe (figure 11). This is not surprising for a material with a high, 600–700 K, Kondo temperature. At low temperatures ($T \leqslant 20$ K) $YbAl_3$ exhibits a region of negative thermal expansion, $\alpha_{[100]}(T) < 0$. For $Yb_{0.1}Lu_{0.9}Al_3$ the region of negative thermal expansion does not appear (above 1.8 K) since $\alpha_{[100]}(T)$ is apparently dominated by the contribution from the $LuAl_3$ matrix. Both

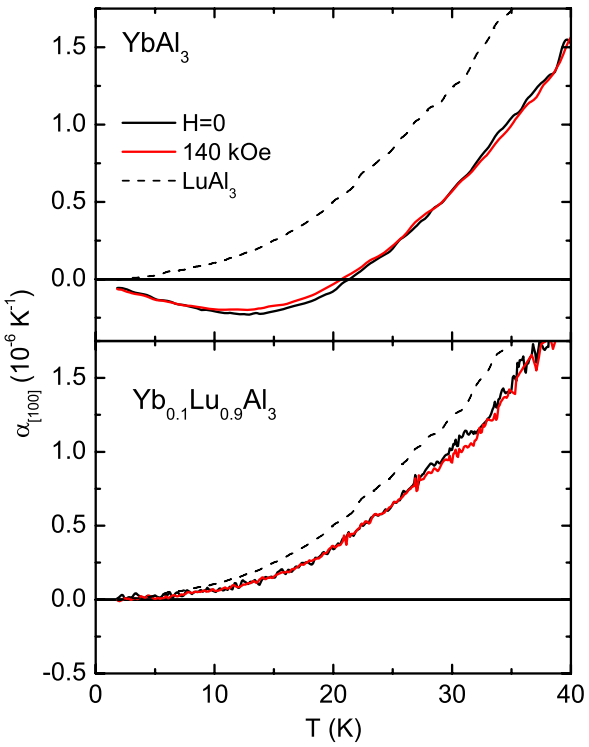

Figure 11. Low temperature part of the linear thermal expansion coefficient for $YbAl_3$ and $Yb_{0.1}Lu_{0.9}Al_3$ in applied fields of 0 and 140 kOe. For comparison, data for $LuAl_3$ are shown as a dashed line.

in pure $YbAl_3$ and in diluted $Yb_{0.1}Lu_{0.9}Al_3$, the temperature dependent thermal expansion is below that for the non-magnetic analog, $LuAl_3$, consistently with an intermediate valence character of the Yb ion in pure and diluted material.

3.2. Magnetostriction and quantum oscillations

In $LuAl_3$ the base temperature (1.8 K) magnetostriction is rather small; however, starting at fields below 40 kOe de Haas–van Alphen (dHvA)-like oscillations in magnetostriction (figure 12) are clearly observed. A fast Fourier transform was performed on these data in the form of $\Delta L/L_0$ versus $1/H$. Seven dHvA frequencies ranging from ∼1 to ∼50 MG were observed (figure 12, inset). The occurrence of quantum oscillations in magnetostriction is a known phenomenon [25]; however observations of such oscillations are rather rare, since both large, high quality single crystals and sensitive dilatometers are required. dHvA oscillations were observed in $LuAl_3$ via magnetostriction up to temperatures as high as 20 K (figure 13). The temperature dependence of the amplitude of these oscillations can be used to evaluate the effective masses of the quasiparticles on the corresponding extremal orbits using the standard Lifshitz–Kosevich formula [26–28]. The obtained dHvA frequencies and corresponding effective masses, m^*/m_0, together with the literature data [29] obtained by a conventional magnetic susceptibility field-modulation technique, are shown in figure 14. Of the seven orbits observed in this work, four (above 10 MG) are consistent with experimental or theoretical literature data and three frequencies ($F < 10$ MG, $m^*/m_0 < 0.5$) are new.

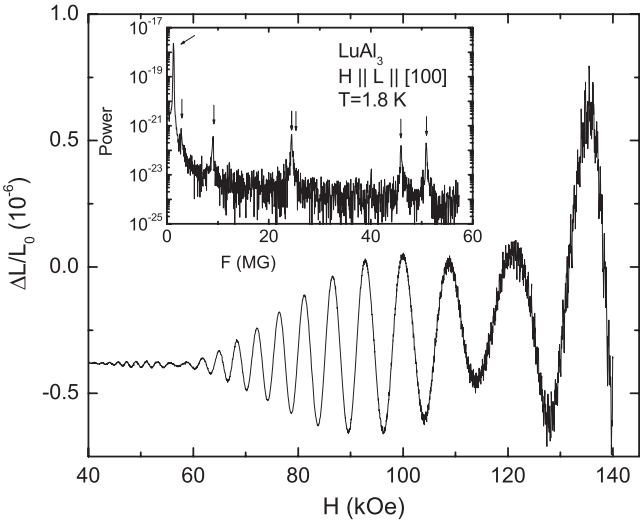

Figure 12. High field part of longitudinal ($H \parallel L \parallel [100]$) magnetostriction in $LuAl_3$ measured at 1.8 K. Inset: fast Fourier transform of the corresponding $\Delta L/L_0$ versus $1/H$ data. Arrows mark the de Haas–van Alphen frequencies.

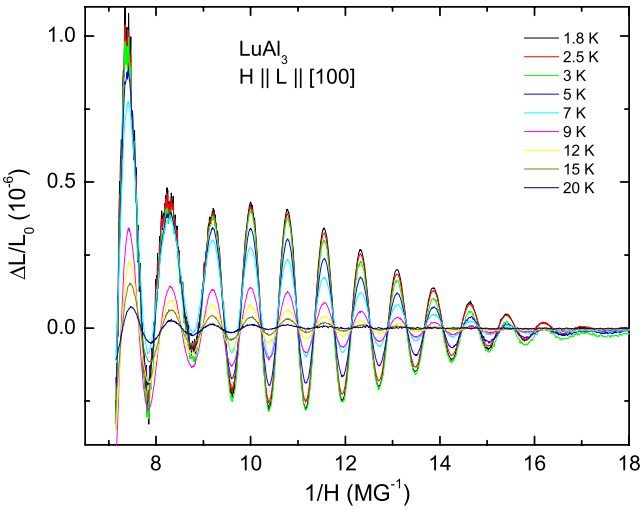

Figure 13. Longitudinal magnetostriction in $LuAl_3$ for $H \parallel [100]$ at different temperatures, from 1.8 to 20 K, plotted as a function of $1/H$. A constant background was subtracted from the data.

The magnetostriction of $YbAl_3$ is also rather small: $\Delta L/L_0 \approx 3 \times 10^{-9}$ at $T = 1.8$ K, $H = 140$ kOe. In high fields dHvA-like oscillations are also observed (figure 15). The amplitude of the oscillations is significantly smaller (few orders of magnitude for the leading frequency) than that for $LuAl_3$ and they reduce to the level of noise above ∼15 K. Two frequencies and their effective masses were identified from our measurements and the results are plotted together with the literature data in figure 16. It is worth noting that, for the orbits detected by means of magnetostriction, the electronic masses in $YbAl_3$ are similar to those found for $LuAl_3$. Significant mass enhancement appears to occur only for higher frequencies.

The longitudinal magnetostriction of $TmAl_3$ is orders of magnitude higher than that of $YbAl_3$ and $LuAl_3$: $\Delta L/L_0 \approx 7 \times 10^{-4}$ at $T = 1.8$ K, $H = 140$ kOe (figure 17).

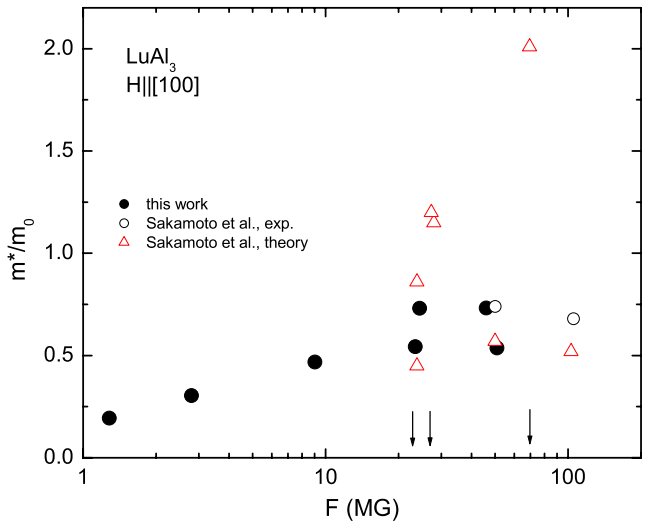

Figure 14. dHvA frequencies and corresponding effective masses for $LuAl_3$, $H \parallel [100]$. Filled circles—this work, other symbols—literature data [29]: open circles—experiment, triangles—theory. Note that Sakamoto *et al* experimentally identified several other dHvA frequencies but did not determine the corresponding effective masses. These experimental frequencies are shown by arrows.

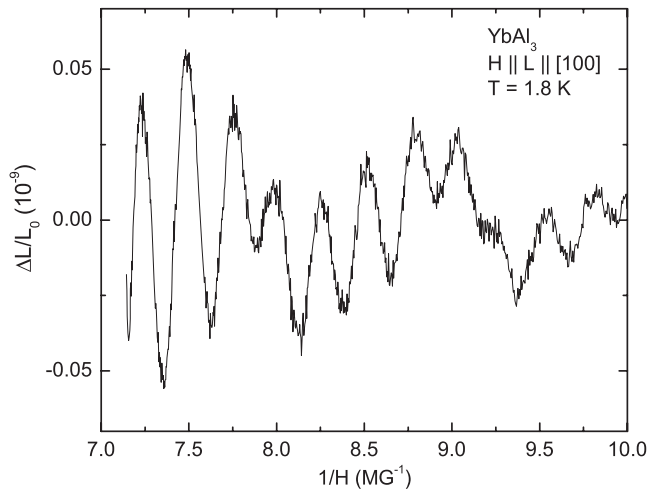

Figure 15. Longitudinal magnetostriction in $YbAl_3$ for $H \parallel [100]$ at $T = 1.8$ K plotted as a function of $1/H$. A constant background was subtracted from the data.

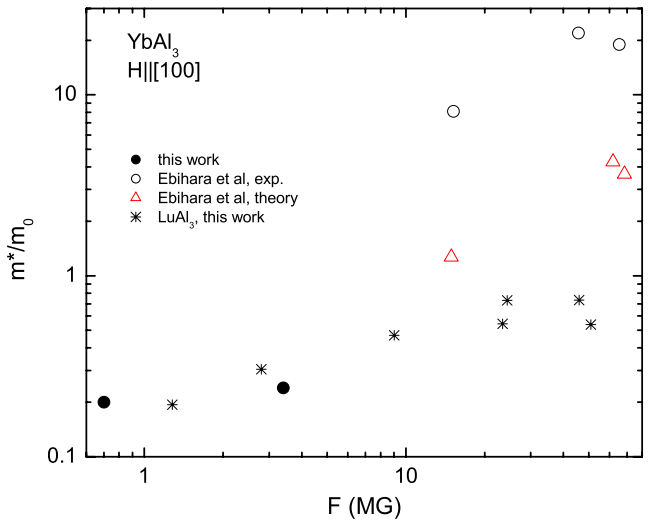

Figure 16. dHvA frequencies and corresponding effective masses for $YbAl_3$, $H \parallel [100]$. Filled circles—this work, other symbols—literature data: open circles—experiment [30], triangles—theory [31]. Data for $LuAl_3$ (this work) are shown as asterisks for comparison.

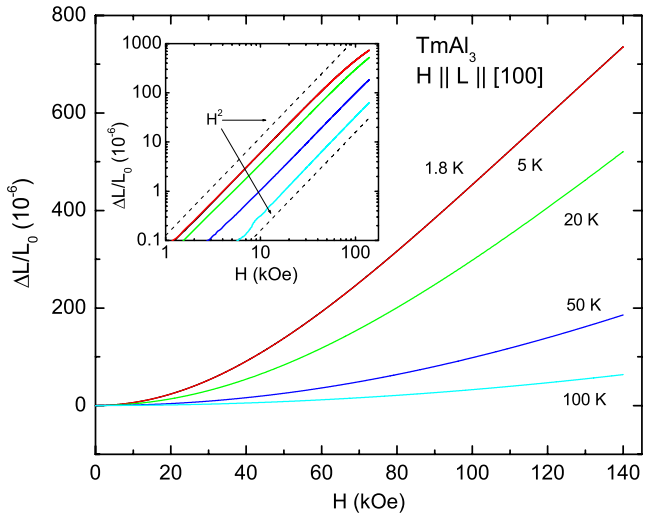

Figure 17. Longitudinal magnetostriction in $TmAl_3$ for $H \parallel [100]$ at different temperatures, from 1.8 to 100 K. Note that within the scale of the plot, 1.8 and 5 K data coincide. Inset: the same data on a log–log plot. Dashed lines correspond to $\Delta L/L_0 \propto H^2$ functional behavior.

In the intermediate and high fields the magnetostriction is approximately proportional to H^2 (figure 17, inset). Detailed analysis of the magnetostriction [32–34] requires knowledge of the details of the Tm^{3+} ion–lattice interactions.

We cannot resolve quantum oscillations of magnetostriction in $TmAl_3$, although there are no indications of inferior crystal quality. We need to mention though that the much higher, monotonic magnetostriction background makes observation of quantum oscillations extremely difficult. Using a traditional magnetic susceptibility modulation technique seven fundamental dHvA frequencies were observed in $TmAl_3$ for $H \parallel [100]$ [35], these frequencies being similar to the ones found for $LuAl_3$ and $YbAl_3$.

4. Summary

Temperature dependent thermal expansion coefficients were measured between 1.87 and 300 K for RAl_3 (R = Lu, Yb, Tm) along the [100] direction. In $YbAl_3$ the intermediate valence of the Yb ions results in $\alpha(T)$ for this material being consistently lower than $\alpha(T)$ for the non-magnetic analog, $LuAl_3$, with a negative thermal expansion region at low temperatures. The thermal expansion coefficient, $\alpha(T)$, of $TmAl_3$ manifests contributions from the CEF effects and, unlike $YbAl_3$ and $LuAl_3$, displays strong field dependence below ~100 K.

The magnetostriction of $YbAl_3$ and $LuAl_3$ ($H \parallel L \parallel [100]$) shows clear dHvA-like oscillations up to temperatures

as high as above 20 K for $LuAl_3$. Several new dHvA frequencies were measured (three for $LuAl_3$ and two for $YbAl_3$) and their effective masses were estimated. For these orbits the electronic masses in $YbAl_3$ are similar to those found for $LuAl_3$. $TmAl_3$ shows very large, exceeding that of $YbAl_3$ and $LuAl_3$ by several orders of magnitude, magnetostriction at low temperatures.

In addition, a CEF splitting scheme for $TmAl_3$ with the Γ_2 level as the ground state is strongly suggested on the basis of the analysis of the heat capacity to significantly higher fields and temperatures. This result removes a two-decade ambiguity as to the CEF level scheme for this material.

Acknowledgments

The work at Ames Laboratory was supported by the US Department of Energy—Basic Energy Sciences under contract no. DE-AC02-07CH11358. GMS was supported by the National Science Foundation under grant DMR-0704406. GMS also gratefully acknowledges the use of the SIMWAP analysis protocol.

References

[1] van Vucht J H N and Buschow K H J 1965 *J. Less-Common Met.* **10** 98
[2] Bargouth M O and Will G 1971 *Phys. Lett.* A **36** 50
[3] Buschow K H J 1965 *Z. Phys. Chem.* **59** 21
[4] Deutz A F, Brom H B, Huiskamp W J, de Jongh L J and Buschow K H J 1989 *Physica* B **160** 83
[5] Havinga E E, Buschow K H J and van Daal H J 1973 *Solid State Commun.* **13** 621
[6] Hiess A, Boucherle J X, Givord F and Canfield P C 1995 *J. Alloys Compounds* **224** 33
[7] Hiess A, Boucherle J X, Givord F, Schweizer J, Lelievre-Berna E, Tasset F, Gillon B and Canfield P C 2000 *J. Phys.: Condens. Matter* **12** 829
[8] Ebihara T, Bauer E D, Cornelius A L, Lawrence J M, Harrison N, Thompson J D, Sarrao J L, Hundley M F and Uji S 2003 *Phys. Rev. Lett.* **90** 166404
[9] Bauer E D, Booth C H, Lawrence J M, Hundley M F, Sarrao J L, Thompson J D, Riseborough P S and Ebihara T 2004 *Phys. Rev.* B **69** 125102
[10] Christianson A D, Fanelli V R, Lawrence J M, Goremychkin E A, Osborn R, Bauer E D, Sarrao J L, Thompson J D, Frost C D and Zarestky J L 2006 *Phys. Rev. Lett.* **96** 117206
[11] Cornelius A L, Lawrence J M, Ebihara T, Riseborough P S, Booth C H, Hundley M F, Pagliuso P G, Sarrao J L, Thompson J D, Jung M H, Lacerda A H and Kwei G H 2002 *Phys. Rev. Lett.* **88** 117201
[12] Iandelli A and Palenzona A 1972 *J. Less-Common Met.* **29** 293
[13] Bucher E, Maita J P, Hull G W Jr, Sierro J, Chu C W and Luthi B 1974 *Proc. 1st Conf. on Cryst. Elec. Field Effects in Metals and Alloys (Montreal)* ed R A V Devine, p 221
[14] de Wijn H W, van Diepen A M and Buschow K H J 1970 *Phys. Rev.* B **1** 4203
[15] Sugiyama K, Futoh M, Iizuka T, Ebihara T, Inoue T, Kindo K and Ōnuki Y 2001 *J. Phys. Soc. Japan* **70** 3753
[16] Canfield P C and Fisk Z 1992 *Phil. Mag.* B **65** 1117
[17] Schmiedeshoff G M, Lounsbury A W, Luna D J, Tracy S J, Schramm A J, Tozer S W, Correa V F, Hannahs S T, Murphy T P, Palm E C, Lacerda A H, Bud'ko S L, Canfield P C, Smith J L, Lashley J C and Cooley J C 2006 *Rev. Sci. Instrum.* **77** 123907
[18] Barron T H K and White G K 1999 *Heat Capacity and Thermal Expansion at Low Temperatures* (New York: Kluwer–Academic/Plenum)
[19] Kroeger F R and Swenson C A 1977 *J. Appl. Phys.* **48** 853
[20] Pott R, Schefzyk R, Wohlleben D and Junod A 1981 *Z. Phys.* B **44** 17
[21] Wohlleben D K 1981 *Valence Fluctuations in Solids* ed L M Falicov, W Hanke and M B Maple (Amsterdam: North-Holland) p 1
[22] Sales B C and Wohlleben D K 1975 *Phys. Rev. Lett.* **35** 1240
[23] Lea K R, Leask M J M and Wolf W P 1962 *J. Phys. Chem. Solids* **23** 1381
[24] Urbano R R, Bittar E M, Pires M A, Mendonça Ferreira A L, Bufaiçal L, Rettori C, Pagliuso P G, Magill B, Oseroff S B, Thompson J D and Sarrao J L 2007 *Phys. Rev.* B **75** 045107
[25] Chandrasekhar B S and Fawcett E 1971 *Adv. Phys.* **20** 775
[26] Lifshitz I M and Kosevich A M 1954 *Dokl. Akad. Nauk SSSR* **96** 963
[27] Lifshitz I M and Kosevich A M 1955 *Zh. Eksp. Teor. Fiz.* **29** 730
Lifshitz I M and Kosevich A M 1956 *Sov. Phys.—JETP* **2** 636 (Engl. Transl.)
[28] Shoenberg D 1984 *Magnetic Oscillations in Metals* (Cambridge: Cambridge University Press)
[29] Sakamoto I, Chen G F, Ohara S, Harima H and Maruno S 2001 *J. Alloys Compounds* **323/324** 623
[30] Ebihara T, Uji S, Terakura C, Terashima T, Yamamoto E, Haga Y, Inada Y and Onuki Y 2000 *Physica* B **281/282** 754
[31] Ebihara T, Inada Y, Murakawa M, Uji S, Terakura C, Terashima T, Yamamoto E, Haga Y, Ōnuki Y and Harima H 2000 *J. Phys. Soc. Japan* **69** 895
[32] Nicholson K, Häfner U, Müller-Hartmann E and Wohlleben D 1978 *Phys. Rev. Lett.* **41** 1325
[33] Campbell I A, Creuset G and Sanchez J 1979 *Phys. Rev. Lett.* **43** 234
[34] Creuset G and Campbell I A 1981 *Phys. Rev.* B **23** 3375
[35] Ebihara T, Aoki D, Inada Y, Settai R, Sugiyama K, Haga Y and Onuki Y 2001 *J. Magn. Magn. Mater.* **226–230** 101